Transforming Sensory Cues into Aversive Emotion via Septal-Habenular Pathway

Highlights

- A bottom-up multimodal sensory pathway via MS mediates sensory-evoked aversion

- MS receives input from PCG and its glutamatergic projection to LHb elicits aversion

- The converging GABAergic projection from MS to LHb antagonizes aversion

- The glutamatergic MS projection to POA enhances locomotion, which facilitates evasion

Authors

Guang-Wei Zhang, Li Shen,
Wen Zhong, Ying Xiong, Li I. Zhang,
Huizhong W. Tao

Correspondence

yxiong@tmmu.edu.cn (Y.X.),
liizhang@usc.edu (L.I.Z.),
htao@usc.edu (H.W.T.)

In Brief

Zhang et al. reveal a circuit for processing innately aversive sensory signals, with glutamatergic projections from MS to LHb and POA to generate the emotional and a motional effect, respectively. This role of MS in mediating aversion is previously unrecognized.

Transforming Sensory Cues into Aversive Emotion via Septal-Habenular Pathway

Guang-Wei Zhang,[1,2] Li Shen,[2,3] Wen Zhong,[2] Ying Xiong,[1,*] Li I. Zhang,[2,3,*] and Huizhong W. Tao[2,3,4,*]

[1]Department of Neurobiology, Chongqing Key Laboratory of Neurobiology, Third Military Medical University, 30 Gaotanyan St., Chongqing 400038, China
[2]Zilkha Neurogenetic Institute, Keck School of Medicine, University of Southern California, Los Angeles, CA 90089, USA
[3]Department of Physiology and Neuroscience, Keck School of Medicine, University of Southern California, Los Angeles, CA 90089, USA
[4]Lead Contact
*Correspondence: yxiong@tmmu.edu.cn (Y.X.), liizhang@usc.edu (L.I.Z.), htao@usc.edu (H.W.T.)
https://doi.org/10.1016/j.neuron.2018.07.023

SUMMARY

Emotions evoked by environmental cues are important for animal survival and life quality. However, neural circuits responsible for transforming sensory signals to aversive emotion and behavioral avoidance remain unclear. Here, we found that medial septum (MS) mediates aversion induced by both auditory and somatosensory stimuli. Ablation of glutamatergic or GABAergic MS neurons results in impaired or strengthened aversion, respectively. Optogenetic activation of the two cell types results in place avoidance and preference, respectively. Cell-type-specific screening reveals that glutamatergic MS projections to the lateral habenula (LHb) are responsible for the induction of aversion, which can be antagonized by GABAergic MS projections to LHb. Additionally, the sensory-induced place avoidance is facilitated by enhanced locomotion mediated by glutamatergic MS projections to the preoptic area. Thus, MS can transmit innately aversive signals via a bottom-up multimodal sensory pathway and produce concurrent emotional and motional effects, allowing animals to efficiently avoid unfavorable environments.

INTRODUCTION

The mammalian central nervous system possesses complicated circuits for generating various emotions and associated behaviors depending on the valence of environmental signals (Etkin et al., 2015; LeDoux, 2012). Aversive sensory stimuli evoke negative emotions, which cause animal avoidance from the experienced environment/context. For brain circuits relevant to processing aversive and reward signals, previous studies have mostly been focused on top-down mechanisms (Berridge and Kringelbach, 2015; Hu, 2016; Lammel et al., 2014). How innately aversive sensory signals are processed and transformed into negative emotions and behavioral avoidance has been largely unclear.

For motivation-directed behaviors, recent studies have suggested that the lateral habenula (LHb) plays a critical role in encoding negative valence and driving avoidance behavior (Baker et al., 2016; Hikosaka, 2010; Namboodiri et al., 2016; Proulx et al., 2014). LHb neurons are responsive to aversive events (Matsumoto and Hikosaka, 2009; Wang et al., 2017). They directly innervate midbrain GABAergic neurons and indirectly inhibit dopaminergic cells (Stamatakis and Stuber, 2012). These findings have supported a notion that LHb is a brain center encoding aversion mostly through inhibition of the reward system (Ji and Shepard, 2007). LHb receives inputs broadly from a variety of brain regions, including the prefrontal cortex, basal ganglia, hypothalamus, and basal forebrain (Kim and Lee, 2012; Namboodiri et al., 2016; Golden et al., 2016; Stephenson-Jones et al., 2016). Recently, some of these inputs to LHb, e.g., the lateral hypothalamus (Lecca et al., 2017) and lateral preoptic area (Barker et al., 2017), have been shown to respond to aversive stimulation, such as foot shocks, and drive aversion. However, how sensory signals reach LHb through different sensory pathways remains poorly studied in general.

In this study, we found that the glutamatergic MS projection to LHb plays an important role in mediating aversive sensory-induced place avoidance. MS receives bottom-up aversive sensory inputs of different modalities via the pontine central gray (PCG) and transmits these signals to LHb to produce aversive emotion and avoidance. These effects can be antagonized by the GABAergic MS projection to LHb. In addition, the glutamatergic MS projection to the preoptic area (POA) promotes locomotion, which facilitates efficient avoidance from non-preferred environments upon initial contacts. Our data highlight a previously unrecognized functional role of MS in transforming innately aversive sensory signals into negative emotions and behavioral avoidance, achieved through a bottom-up multisensory pathway leading up to LHb.

RESULTS

MS Mediates Sensory-Induced Aversion

To study aversive emotion induced by sensory cues, we exploited a two-compartment real-time place preference test (Stamatakis and Stuber, 2012; Zhu et al., 2016; Lecca et al., 2017) (see STAR Methods). In a test box containing two chambers equally novel to the mouse, we applied potentially aversive
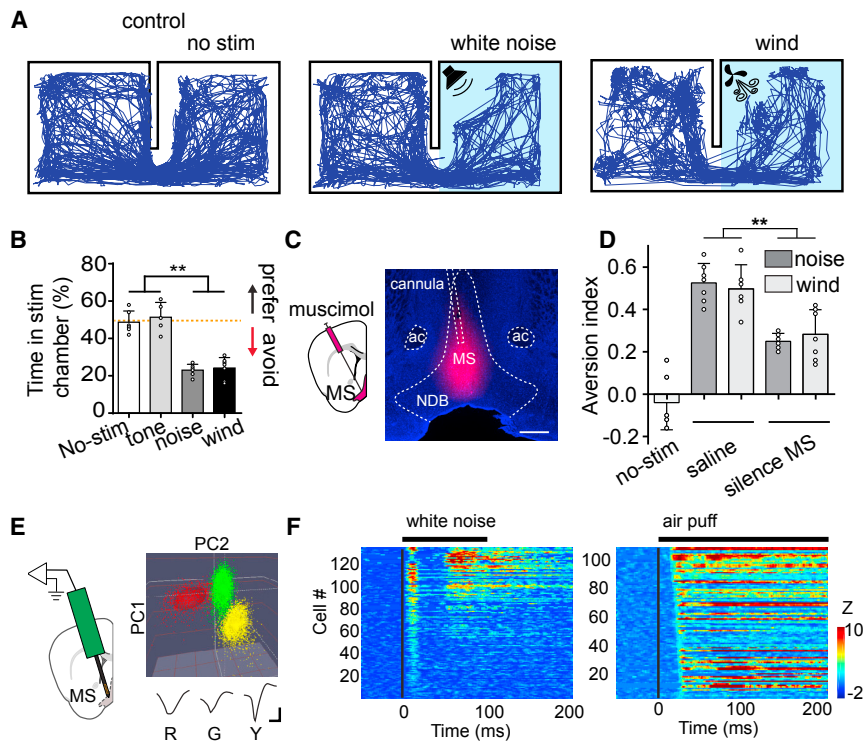
Figure 1. MS Mediates Sensory-Induced Place Aversion

(A) Representative movement tracking traces in the two-chamber place preference test. Left: no stimulation was applied. Middle and right: high-intensity noise or wind blow was applied in the stimulation chamber.

(B) Summary of percentage time spent in the stimulation chamber during the test session. Red dash line marks 50% level. n = 6, 5, 6, and 7 animals for no stimulation, tone, noise, and wind-blow groups, respectively. All error bars in this figure indicate SD. **p < 0.01, one-way ANOVA with post hoc test.

(C) Infusion of fluorescent muscimol into MS. Confocal image shows the restricted spread of muscimol within MS. Scale bar, 500 μm. NDB, nucleus of diagonal band; ac, anterior commissure.

(D) Summary of aversion index in no-stimulation control, saline-injected control, and MS silencing (with muscimol) groups. Aversion index was calculated as the fraction of time spent in the control chamber minus that in the stimulation chamber. n = 5, 7, 6, 6, and 7 mice, respectively. **p < 0.01, one-way ANOVA with post hoc test.

(E) Single-unit recording in MS with a 16-channel probe. Color graph depicts three single units identified by principal-component analysis. Their corresponding average spike waveforms are shown below. R, red; G, green; Y, yellow. Scale bar, 20 μV, 0.5 ms.

(F) Heatmap plotting of Z score for spike responses of MS neurons to noise (left) and air puffs (right). Each row represents one neuron. The black line above indicates the duration of sound or air-puff stimulation (onset is at time zero).

stimuli of different modalities, such as high-intensity (80 dB sound pressure level [SPL]) white noise sound from a speaker and wind blows from a fan, in one of the chambers (designated as the stimulation chamber) (Figure 1A). These stimuli resulted in animals' avoidance of the stimulation chamber, as demonstrated by the relatively less amount of time spent in that chamber within a 20-min test session, whereas the mice spent equal amount of time in each chamber when no stimulus was applied (Figures 1A and 1B; Figure S1). The noise-induced avoidance may not be obvious in a single-chamber test (Fadok et al., 2017). Interestingly, in contrast to noise, pure tones (10 kHz, 80 dB SPL) failed to induce place avoidance in the two-chamber test (Figure 1B).
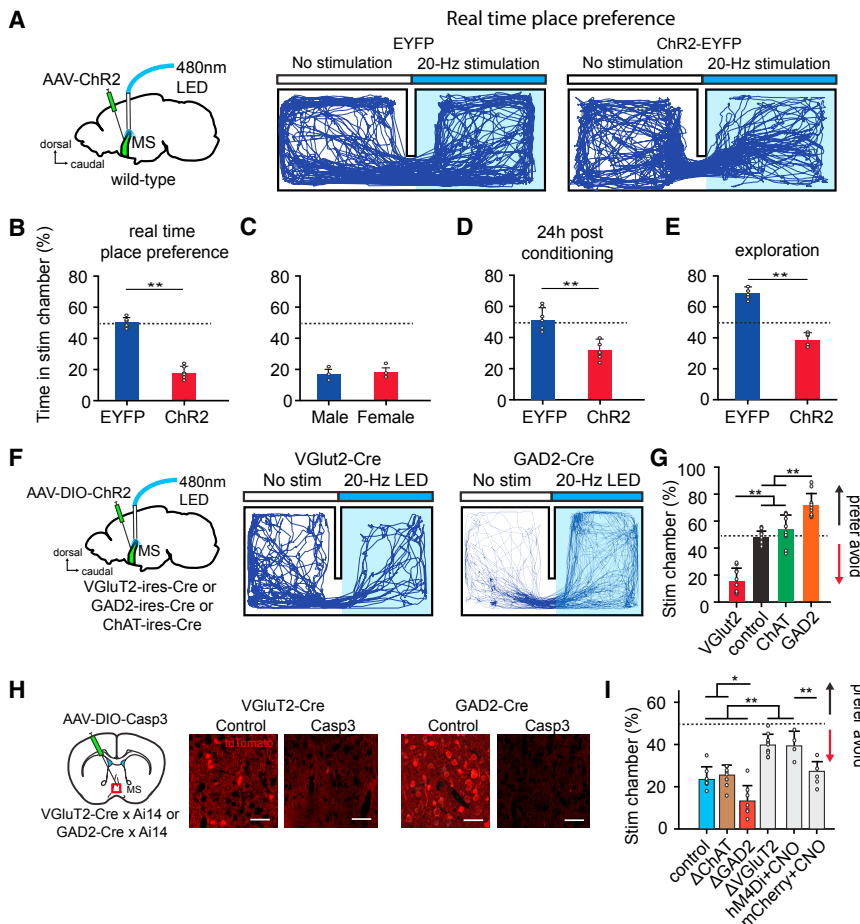
The limbic system is known to be involved in emotional functions (Kringelbach, 2016). Recently, we have discovered that a reticular-limbic auditory pathway via the medial septum (MS) in the basal forebrain transmits specifically noise instead of tone signals (Zhang et al., 2018). In freely moving animals, we confirmed that MS neurons responded much more strongly to noise than pure tones (Figure S2A). In addition, the MS is multisensory, since both sound- and touch-evoked activity has been reported in this structure (Mercer and Remley, 1979; Miller and Freedman, 1993). All these findings have raised an interesting hypothesis that MS might be involved in the observed sensory evoked avoidance behavior. To test this possibility, we silenced MS activity by infusing muscimol (Fig-

ure 1C; see STAR Methods). This significantly reduced the avoidance behavior induced by the natural sensory stimuli of noise and wind blow, whereas saline infusion had no effect (Figure 1D). These results indicate that MS does play a role in mediating the place avoidance evoked by aversive sensory stimuli.

We next examined MS responses to noise and air puffs by performing single-unit recordings with a multi-channel probe in awake head-fixed mice (Figure 1E; Figure S2B), which were placed on a smoothly rotatable running plate (see STAR Methods). We confirmed that MS neurons could be activated by 80 dB SPL noise or air puff stimulation (Figure 1F; Figure S2C). Out of 134 MS neurons, 17.3% only responded to noise, 15.4% only responded to air puffs, and 67.3% responded to both noise and air puffs, using a criterion of Z score > 3 (Figure S2D; see STAR Methods). Therefore, the majority of MS neurons are multisensory and can be activated by more than one type of aversive sensory stimulation.

MS Activation Induces Place Aversion

To directly test the behavioral effect of MS activation, we optogenetically stimulated MS neurons by injecting adeno-associated virus (AAV) expressing channelrhodopsin2 (ChR2) (Boyden et al., 2005). A train of LED pulses (20-ms duration) was delivered through an implanted optic fiber to activate ChR2-expressing MS neurons whenever the animal was in the designated

Figure 2. Activation of Glutamatergic MS Neurons Induces Aversion

(A) Movement tracking traces for an EYFP control and a ChR2-expressing mouse for which optogenetic activation of MS neurons was applied (marked by blue bar).

(B) Percentage time spent in the stimulation chamber for EYFP control (n = 6) and ChR2-expressing (n = 6) mice. All error bars in this figure indicate SD. **p < 0.01, t test.

(C) Comparison of percentage time spent in the stimulation chamber between ChR2-expressing male (n = 3) and female (n = 3) mice. p > 0.5, t test.

(D) Percentage time spent in the stimulation chamber tested 24 hr after conditioning (with LED simulation) the animal to the stimulation chamber. n = 6 and 6 mice for EYFP control and ChR2 groups, respectively.

(E) Percentage time spent in the stimulation chamber tested after habituating the animal in the home chamber for 20 min. n = 5 and 5 mice for EYFP control and ChR2 groups, respectively.

(F) Movement tracking traces for a VGluT2-Cre and GAD2-Cre animal expressing ChR2 for which optogenetic stimulation of glutamatergic and GABAergic MS neurons was applied, respectively.

(G) Percentage time spent in the stimulation chamber for mice expressing ChR2 (red, n = 9) or EYFP (black, n = 10) in glutamatergic MS neurons or expressing ChR2 in cholinergic (green, n = 9) or GABAergic (orange, n = 9) MS neurons. Bar, SD. **p < 0.01, one-way ANOVA with post hoc test.

(H) Cell-type-specific ablation by injecting AAV encoding Cre-dependent caspase-3. Fluorescence images show labeled cell types 2 weeks after the injection. Scale bar, 50 μm.

(I) Percentage time spent in the stimulation chamber (noise applied) for EYFP control (n = 7); mice in which cholinergic (n = 7), GABAergic (n = 7), or glutamatergic (n = 8) MS neurons were ablated; and mice expressing hM4Di (n = 5) or mCherry (n = 4) in glutamatergic neurons MS with CNO injected (i.p., 1 mg/kg). *p < 0.05, **p < 0.01, one-way ANOVA with post hoc test.

stimulation chamber (Figure 2A; Figure S3A). Since 10–20 Hz firing rates were the most frequently observed firing rates evoked by noise in MS neurons (Figure S2C), we mostly used 20-Hz LED stimulation. Mice expressing EYFP only served as control. While control mice spent about equal amount of time in each chamber, the ChR2-expressing animals spent less time in the stimulation than the control chamber (Figures 2A and 2B). Male and female mice exhibited similar behaviors (Figure 2C). LED simulation at lower frequencies generated weaker behavioral effects (Figure S3B). These results suggest that directly stimulating the MS signaled negative motivational valence similar to aversive sensory stimulation. In addition, after repeated stimulation of the MS with the animal confined in the designated stimulation chamber (20-min session, one session per day for two consecutive days), the animal spent less time in the stimulation than the control chamber on the following testing day even though no LED stimulation was applied (Figure 2D; Figure S3C). Therefore, the animal had learned the association between the context and the negative effects of MS stimulation and exhibited conditioned place aversion.

We also applied a slightly different place preference test. After the animal was habituated to the designated home chamber for 20 min, the gate leading to the other (novel) chamber was opened. LED stimulation was delivered to activate MS whenever the animal entered and stayed in the novel chamber. Within a 20-min test session following the gate opening, EYFP control animals spent more time in the novel than the home chamber (Figure 2E), consistent with the notion that animals prefer unfamiliar than familiar environments (Crawley, 1985; Vankov et al., 1995). However, ChR2-expressing animals spent less time in the novel chamber (Figure 2E), further strengthening the conclusion that MS activation results in place avoidance. Together, our behavioral experiments confirm that MS activation signals negative valence.

Involvement of Glutamatergic MS Neurons in Aversion

The MS contains three major neuronal types: GABAergic, cholinergic, and glutamatergic (Colom et al., 2005; Freund and Antal, 1988; Justus et al., 2017; Saunders et al., 2015; Xu et al., 2015). To understand which type of MS neuron mediates the naturally induced avoidance behavior, we injected AAV encoding Cre-dependent ChR2 into the MS of GAD2-Cre, ChAT-Cre, or VGluT2-Cre mice to express ChR2 specifically in GABAergic, cholinergic, or glutamatergic neurons, respectively (Figure 2F).

In the same two-chamber real-time place preference test, activating glutamatergic MS neurons caused animal avoidance of the stimulation chamber (17% ± 8%; Figures 2F and 2G), similar to the result of stimulating the MS in the non-cell-type-specific manner. On the contrary, activating GABAergic neurons caused preference of the stimulation chamber (72% ± 7%; Figures 2F and 2G). Stimulating cholinergic neurons, in contrast, did not result in either avoidance or preference (54% ± 9%; Figure 2G). All of these behavioral tests were performed in the dark cycle of animals to avoid ambiguity caused by different levels of baseline locomotion in light and dark cycles (Figures S3D–S3F).

To further confirm the role of the glutamatergic neurons, we injected AAV encoding Cre-dependent caspase-3 (Yang et al., 2013) into the MS of VGluT2-Cre mice. Two weeks after the injection, glutamatergic MS neurons were mostly ablated (Figure 2H). This cell ablation nearly abolished the place avoidance induced by high-intensity noise (Figure 2I, ΔVGluT2). Similarly, chemogenetic silencing of glutamatergic MS neurons by expressing Cre-dependent inhibitory designer receptors exclusively activated by designer drugs, DREADDi (Zhu and Roth, 2014), also greatly impaired the place avoidance induced by noise (Figure 2I, hM4Di + CNO). On the contrary, ablation of GABAergic MS neurons by injecting the caspase-3 virus into GAD2-Cre mice (Figure 2H) enhanced the naturally induced avoidance behavior as compared with EYFP control animals (Figure 2I). Ablation of cholinergic neurons did not significantly affect the avoidance behavior (Figure 2I). Together, these results demonstrate that the glutamatergic neurons primarily mediate the MS-dependent avoidance behavior, whereas the GABAergic neurons may inhibit the behavior.

The MS-to-LHb Pathway Mediates Sensory-Induced Aversion

We next examined downstream targets of MS neurons. In VGluT2-Cre mice injected with AAV encoding Cre-dependent ChR2-EYFP, we found that glutamatergic MS neurons projected strongly to the preoptic area (POA), lateral hypothalamic area (LHA), lateral habenula (LHb) (Figure 3A), the entorhinal cortex (EC; data not shown; also see Justus et al., 2017; Zhang et al., 2018), and relatively sparsely to the hippocampus and medial habenula (MHb) (Figure 3A). GABAergic MS neurons exhibited a similar projection pattern (Figure 3A). Cholinergic MS neurons, however, did not project to POA or hypothalamus but projected profusely to the hippocampus (Figure 3A), consistent with previous reports (Li et al., 2018; Zaborszky et al., 2012), while only sparsely to LHb (Figure 3A).

We then dissected which of these target nuclei was involved in the MS-dependent avoidance behavior by optically stimulating ChR2-expressing axons from glutamatergic MS neurons in different target areas. Notably, stimulating the MS-to-LHb projection resulted in animal avoidance of the stimulation chamber (Figures 3B and 3G), similar to stimulating the MS neuronal cell bodies. MS-to-LHb projections were further confirmed by injecting AAVretro-GFP in LHb, which retrogradely labeled neurons in MS (Figures S4A and S4B). In contrast, stimulating glutamatergic MS projections to other major targets, including POA, LHA, hippocampus (dorsal or ventral), and EC, did not cause avoidance or preference (Figures 3C, 3D, and 3G). The avoidance behavior

induced by optogenetically activating glutamatergic MS neurons disappeared when LHb was silenced by local infusion of muscimol (Figures 3E and 3G), and chemogenetic silencing of the glutamatergic MS-to-LHb pathway greatly reduced the noise-induced avoidance (Figure S4F). On the other hand, chemogenetic inactivation of glutamatergic MS projections to the hippocampus or EC did not significantly affect the sensory-induced aversion (Figures S4C and S4F), arguing against involvements of these pathways.

In contrast to stimulating glutamatergic MS-to-LHb projections, stimulating GABAergic MS-to-LHb projections resulted in place preference (Figures 3F and 3G), which is consistent with the result of stimulating GABAergic MS neuron cell bodies. On the other hand, stimulating GABAergic projections to POA or LHA did not induce either avoidance or preference (Figures S4G–S4I). Chemogenetic inactivation of GABAergic MS projections to the hippocampus or EC did not significantly affect the sensory-induced aversion (Figures S4E and S4F), also excluding involvements of these GABAergic pathways in avoidance behavior. Furthermore, inactivating cholinergic projections to the hippocampus or EC also did not affect the sensory induced aversion (Figures S4D and S4F), further arguing against involvements of cholinergic MS neurons in avoidance behavior. Together, our data demonstrate that MS-dependent aversion is mediated through the glutamatergic MS-to-LHb pathway, which can be antagonized by the GABAergic MS-to-LHb projection. These results are consistent with the role of LHb in signaling events of negative values (Golden et al., 2016; Li et al., 2011; Matsumoto and Hikosaka, 2007; Stamatakis and Stuber, 2012).

Converging and Opposing Glutamatergic and GABAergic MS Projections to LHb

Using single-unit recordings, we revealed that LHb neurons, which are predominantly glutamatergic (Aizawa et al., 2012; Lecca et al., 2014), also responded to high-intensity noise or air puffs (Figure 4A). Compared to the MS, LHb neuron responses were overall delayed by a few milliseconds (Figure 4B; Figures S5A and S5B). In addition, sensory-evoked activity in LHb largely disappeared when the MS was silenced by local infusion of muscimol (Figures 4C and 4D). These results demonstrate a direct sensory pathway from the MS to the LHb, which can process aversive sensory signals.

To further understand the functional connectivity between the MS and the LHb, we carried out whole-cell recordings from LHb neurons in brain slice preparations while optically stimulating ChR2-expressing MS axons in LHb (Figure 4E). Recordings were made in the presence of TTX and 4AP to block polysynaptic responses (Petreanu et al., 2009). Activation of glutamatergic MS axons induced excitatory postsynaptic currents (EPSCs) in LHb neurons, which could be blocked by CNQX, a blocker of glutamate receptors (Figure 4E). On the other hand, activation of GABAergic MS axons elicited inhibitory postsynaptic currents (IPSCs) only, which could be blocked by gabazine, a blocker of GABA$_A$ receptors (Figure 4F). In wild-type animals in which MS neurons expressed ChR2 non-cell-type specifically, LED stimulation evoked both an EPSC and an IPSC in individual LHb neurons (Figure 4G), indicating that single LHb neurons could be
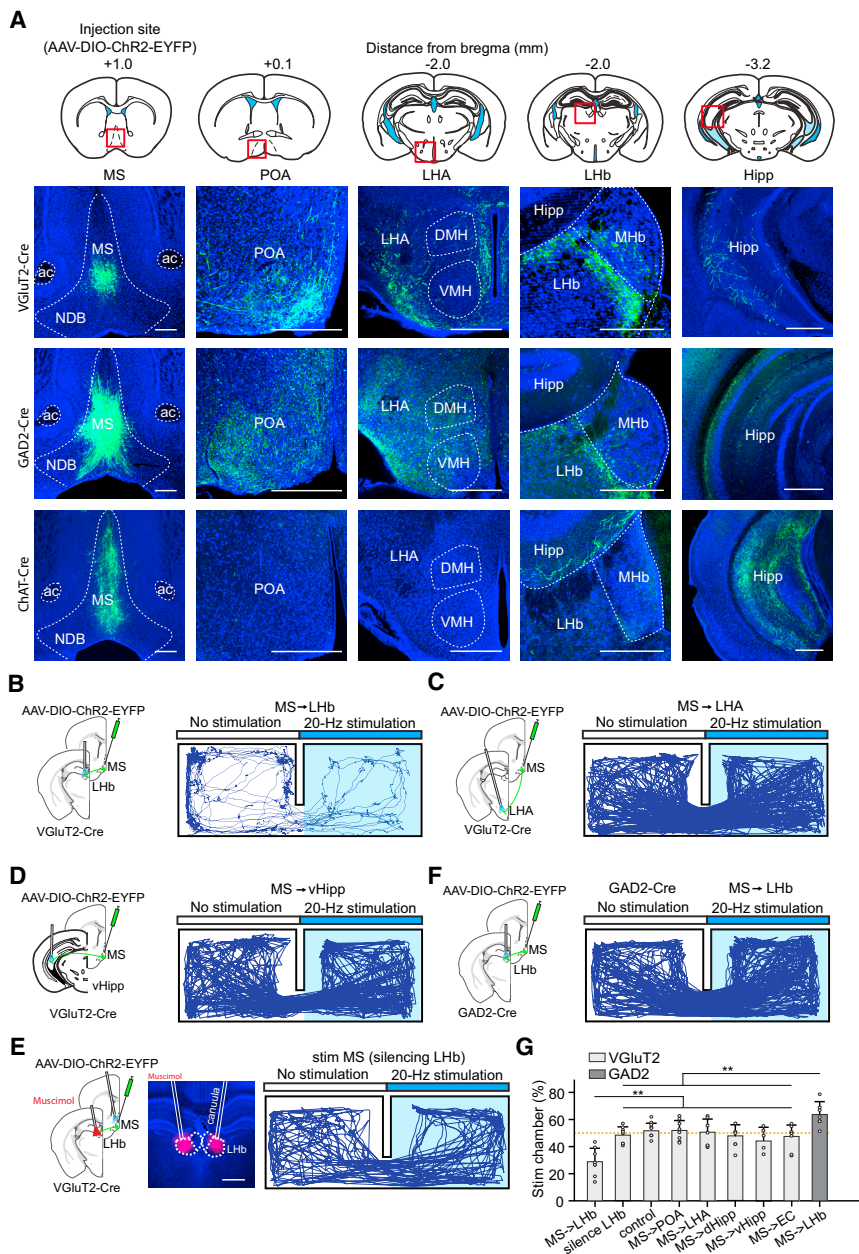
Figure 3. The Glutamatergic MS-to-LHb Projection Mediates the Avoidance Behavior

(A) Projection targets of different types of MS neurons. Injections were made in VGluT2-Cre, GAD2-Cre, and ChAT-Cre mice, respectively. Left column: fluorescence at the injection site. Right four columns: fluorescence-labeled axons in target regions. Scale bar, 500 μm.

(B) Movement tracking traces for an animal in which ChR2-expressing glutamatergic MS axons in LHb were stimulated by LED delivery.

(C) Movement tracking traces for an animal in which ChR2-expressing glutamatergic MS axons in LHA were stimulated.

(D) Movement tracking traces for an animal in which ChR2-expressing glutamatergic MS axons in the ventral hippocampus were stimulated.

(E) Movement tracking traces for an animal in which glutamatergic MS neurons were stimulated while LHb was silenced by muscimol. Image (middle) shows the restricted spread of muscimol within LHb. Scale bar, 500 μm.

(F) Movement tracking for an animal in which ChR2-expressing GABAergic MS axons in LHb were stimulated.

(G) Percentage time spent in the stimulation chamber for different experimental groups: glutamatergic MS-to-LHb projection was stimulated (n = 7); glutamatergic MS neurons were stimulated while LHb was silenced (n = 7); EYFP control (n = 7); glutamatergic MS-to-POA (n = 8), MS-to-LHA (n = 7), MS-to-dorsal hippocampus (n = 5), MS-to-ventral hippocampus (n = 5), or MS-to-entorhinal cortex (n = 5) projection was stimulated; and GABAergic MS-to-LHb projection was stimulated (n = 6). **p < 0.01, one-way ANOVA with post hoc test. Error bars, SD.

gic unit in Figure 4H, blue LED pulses faithfully evoked time-locked spikes. Peri-stimulus spike time histogram (PSTH) for the evoked spikes revealed two peaks, at about 3 ms and 6 ms following the onset of LED pulses, respectively (Figure S5C). The first peak was due to spikes directly activated by LED, while the second was likely due to

innervated by both glutamatergic and GABAergic MS axons. Together, our results demonstrate that glutamatergic and GABAergic MS projections converge onto LHb neurons. This explains why simulating glutamatergic and GABAergic MS neurons separately produced opposite behavioral effects.

Since glutamatergic and GABAergic MS projections converge onto LHb neurons, yet aversive sensory stimulation produced a behavioral effect similar to stimulating glutamatergic MS neurons alone, we wondered whether GABAergic and glutamatergic MS neurons had different sensory responses. To address this issue, we optogenetically identified glutamatergic and GABAergic MS neurons in VGluT2- and GAD2-Cre mice, respectively (see STAR Methods). As shown by an example glutamater-

indirect activation via local excitatory connectivity between MS cells. We used a criterion of Z score > 3 to identify units excited by sensory stimulation. Among these units, glutamatergic neurons were much more strongly activated than GABAergic cells (Figure 4I; Figure S5D). In addition, the spiking of GABAergic neurons was delayed relative to the glutamatergic neurons, as shown by the distribution of first-spike latencies (Figure 4J). This observation is consistent with a previous report in the basal forebrain that GABAergic neurons are innervated by glutamatergic neurons (Xu et al., 2015). The relatively more dominant sensory responses of glutamatergic MS neurons may account for the overall aversive effect behaviorally, which can be generated by the stimulation of glutamatergic neurons alone.
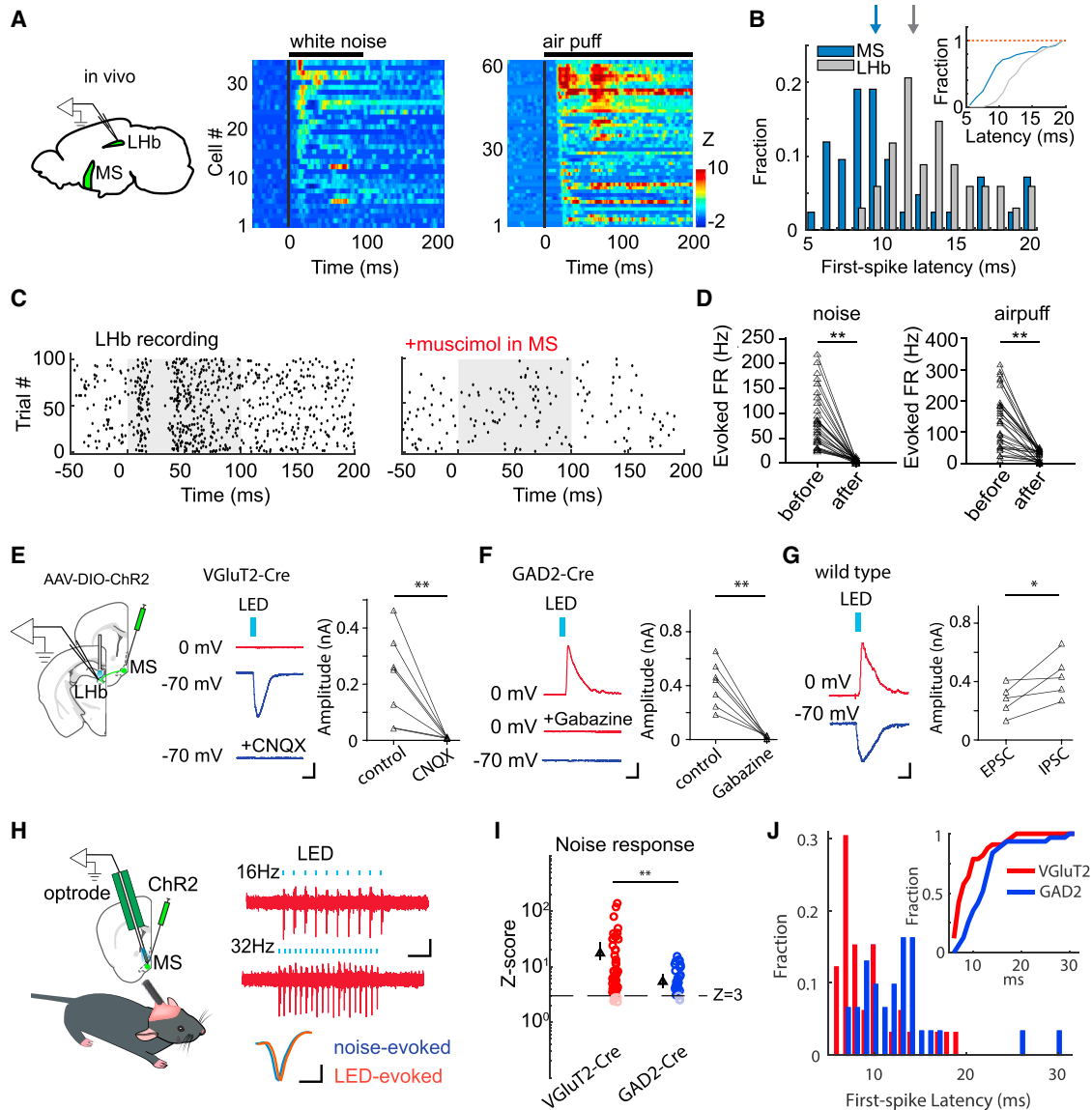
Figure 4. MS to LHb Functional Connectivity and Analysis of Cell Types

(A) Single-unit recordings in LHb. Heatmap plots time-dependent Z score for spike responses of LHb neurons to high-intensity noise or air puffs.

(B) Distribution of first-spike latencies of noise responses in MS and LHb neurons. Inset: cumulative distribution ($p < 0.01$, Kolmogorov-Smirnov test).

(C) Raster plot for spikes of an LHb neuron before and after silencing MS with muscimol. Gray box marks the duration of noise presentation.

(D) Firing rates of LHb neurons (n = 34) evoked by noise (left) or air puffs (right) before and after silencing MS. Data points for the same neuron were connected by a line.

(E) Left: illustration of slice recording from LHb neurons while activating glutamatergic MS axons in LHb. Middle: an example recording in the VGluT2-Cre slice. LED evoked no IPSC at 0 mV but evoked an EPSC at −70 mV, which was blocked by CNQX. Scale bar, 40 pA, 5 ms. Right: summary of EPSC amplitudes of 7 LHb neurons before and after CNQX application. **$p < 0.01$, paired t test.

(F) Left: an example recording in the GAD2-Cre slice. LED evoked an IPSC at 0 mV, which was blocked by gabazine, but no EPSC at −70 mV. Scale bar, 30 pA, 5 ms. Right: IPSC amplitudes of 7 LHb neurons before and after CNQX application. **$p < 0.01$, paired t test.

(G) Left: an example recording in the wild-type slice. LED evoked both an IPSC at 0 mV and an EPSC at −70 mV. Scale bar, 30 pA, 5 ms. Right: comparison of EPSC and IPSC amplitudes in the same cells (n = 5). *$p < 0.05$, paired t test.

(H) Left: optrode recording to identify cell types. Top right: LED evoked spikes of an example glutamatergic MS neuron. Scale bar, 30 μV, 100 ms. Bottom right: average waveforms for noise-evoked (blue) and LED-evoked (red) spikes from the same unit. Note that the waveforms are slightly offset for comparison. Scale bar, 30 μV, 0.5 ms.

(I) Comparison of responsiveness of glutamatergic and GABAergic MS neurons to noise. Peak Z scores are plotted. Dash line marks Z score = 3. Triangle represents the average of Z scores that are >3. **$p < 0.01$, t test, n = 35 and 55. Error bars, SEM.

(J) Distribution of first-spike latencies (in response to noise) of glutamatergic (red) and GABAergic (blue) MS neurons. Inset: cumulative distribution ($p < 0.001$, Kolmogorov-Smirnov test).
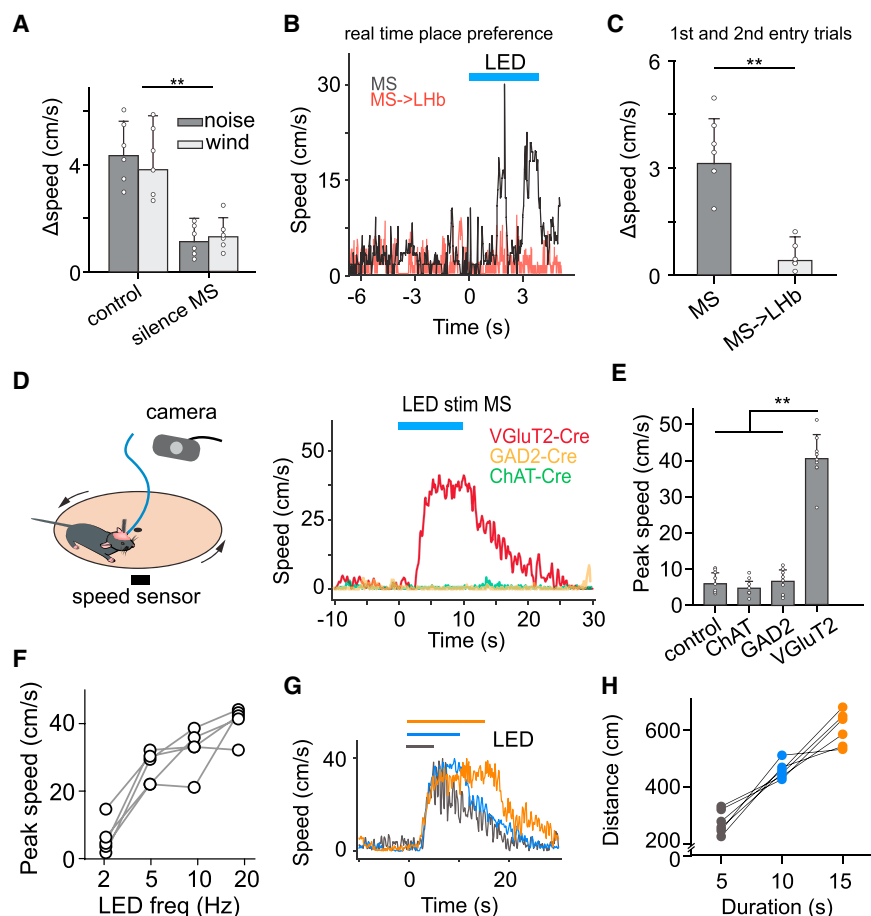
Figure 5. MS Activation Promotes Locomotion

(A) Difference of average speed in the stimulation (noise or wind-blow applied) versus control chamber for control (n = 6) and experimental animals with MS silenced with muscimol (n = 6). **p < 0.01, t test. All error bars in this figure indicate SD.

(B) Plot of locomotion speeds during an entry trial in the real-time place preference test for example animals with MS neuron cell bodies stimulated (gray; see Video S1) or MS-to-LHb axon terminals stimulated (red). Time zero is when the animal entered the stimulation chamber. Blue line marks the duration of LED stimulation.

(C) Difference of average speed in the stimulation versus control chamber for groups with MS neuron cell bodies stimulated (n = 6) or MS-to-LHb axon terminals stimulated (n = 6). **p < 0.01, t test.

(D) Left: head-fixed running test. Right: speed traces for an example animal with glutamatergic (red), GABAergic (orange), or cholinergic (green) MS neurons stimulated. Blue line marks the duration of LED stimulation.

(E) Summary of peak running speed elicited by stimulating distinct types of MS neurons. n = 8, 6, 8, and 8, respectively. **p < 0.01, one-way ANOVA and post hoc test.

(F) Plot of average speed versus of frequency of LED stimulation. Data points from the same animal are connected with lines. n = 5 mice.

(G) Speed traces for an example animal in which glutamatergic MS neurons were stimulated for different durations (marked by colored lines).

(H) Running distances for different stimulation durations. Data points from the same animal are connected.

Locomotion Effect of MS Activation

In the sensory-cued place preference tests, we observed that the average speed of locomotion was higher in the stimulation than in the control chamber and that this difference disappeared when the MS was silenced (Figure 5A). Analysis of video frames revealed that stimulation of glutamatergic MS neuron cell bodies enhanced locomotion speed with a delay, which is consistent with previous observations (Fuhrmann et al., 2015; Hinman et al., 2016), whereas stimulation of glutamatergic MS-to-LHb axon terminals did not apparently affect the speed (Figures 5B and 5C; Video S1). The animals in our cohorts ran normally, exhibiting a range of instantaneous speeds comparable to those in previous studies (e.g., Fuhrmann et al., 2015) (Figures S6A–S6C). These findings suggest that MS activation might produce a locomotion effect independent of its projection to LHb. To further examine this issue, we directly measured locomotion speed in head-fixed animals placed on a running plate (Liang et al., 2015; Xiong et al., 2015) (Figure 5D). Optogenetic activation of glutamatergic MS neurons induced an increase in locomotion speed, whereas activation of GABAergic or cholinergic MS neurons did not have any effect (Figures 5D and 5E). The increase in speed was stronger with higher-frequency LED stimulation (Figure 5F; also see Videos S2, S3, and S4 and Figure S6D) and could persist throughout the LED stimulation (Figure 5G, 5H;

also see Videos S5, S6, and S7 and Figure S6D). These data demonstrate that activation of glutamatergic MS neurons can directly promote locomotion.

The MS-to-POA Projection Promotes Locomotion

We further examined which downstream target of MS might mediate the locomotion effect. By stimulating glutamatergic MS axons in different target regions while silencing the cell bodies with muscimol infusion (Figure 6A), we found that only stimulating the MS-to-POA projection induced an increase in locomotion (Figures 6A and 6B). The latency of the speed increase was comparable to that when MS neuron cell bodies were stimulated (Figure 6C). Silencing POA with muscimol blocked this increase of speed induced by optogenetically activating MS neuron cell bodies (Figure 6B), further suggesting that the locomotion effect is mediated through the MS-to-POA projection.

We next examined the overlap between the MS neuron populations projecting to POA and to LHb by injecting retrograde tracers (AAVretro or CTB) of different colors in POA and LHb, respectively (Figure 6D; Figure S7A). The retrogradely labeled red and green neurons in the MS only sparsely overlapped (Figures 6D and 6E; Figure S7A), suggesting that POA- and LHb-projecting glutamatergic MS neurons are largely separate
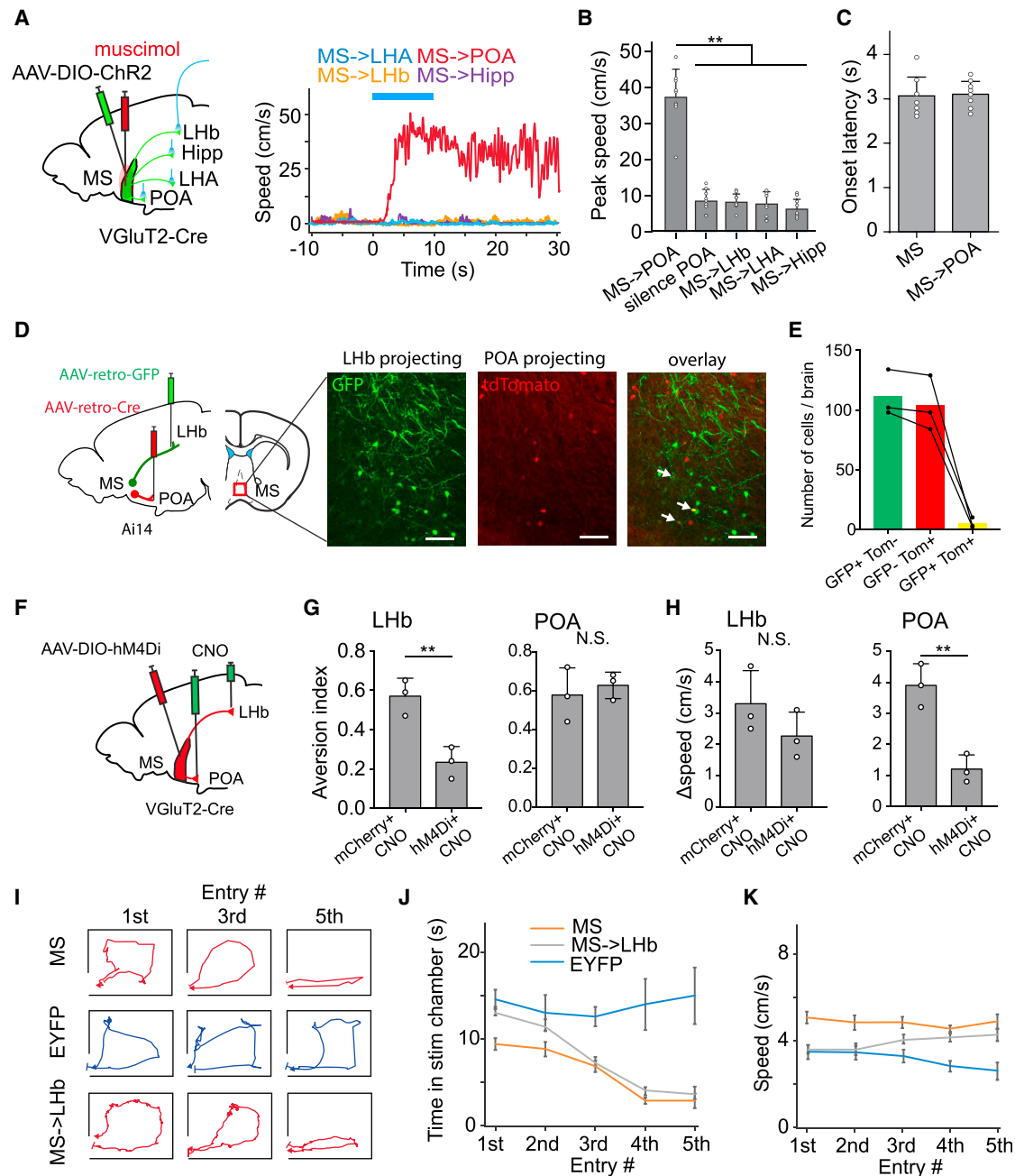
Figure 6. The MS-to-POA Projection Mediates the Locomotion Effect

(A) Left: MS (glutamatergic) projections to different target regions were stimulated. Right: speed traces for example animals with the MS-to-POA (red), MS-to-LHA (blue), MS-to-LHb (orange), or MS-to-hippocampus (purple) projection stimulated. MS was silenced with muscimol.

(B) Summary of peak speeds elicited by stimulating different MS projections. "silence POA," MS neurons were stimulated while POA was silenced. n = 9, 9, 9, 9, and 8, respectively. **p < 0.01, one-way ANOVA and post hoc test. All error bars in this figure indicate SD.

(C) Comparison of onset latency of induced locomotion between stimulating MS neuron cell bodies (n = 8) and MS-to-POA projection (n = 9). p = 0.23, t test.

(D) Labeling of LHb- and POA-projecting MS neurons by injecting different AAVretro in target regions in Ai14 tdTomato reporter mice. Images show GFP-labeled LHb-projecting and tdTomato-labeled POA-projecting neurons in MS. White arrows mark co-labeled neurons. Scale bars, 50 μm.

(E) Number of MS neurons labeled by GFP only (green), tdTomato only (red), or both GFP and tdTomato (yellow) in three animals.

(F) Strategy for projection-specific silencing using DREADDi.

(G) Aversion index for silencing MS axon terminals in LHb (n = 3 and 3 for control and experimental groups, respectively) and POA (n = 3 and 3 for control and experimental groups, respectively). N.S., non-significant. **p < 0.01, t test.

(H) Difference of average speed in the stimulation versus control chamber for mice with glutamatergic MS axon terminals in LHb (n = 3 and 3 for control and experimental groups, respectively) or POA (n = 3 and 3 for control and experimental groups, respectively) were chemogenetically silenced. **p < 0.01, t test.
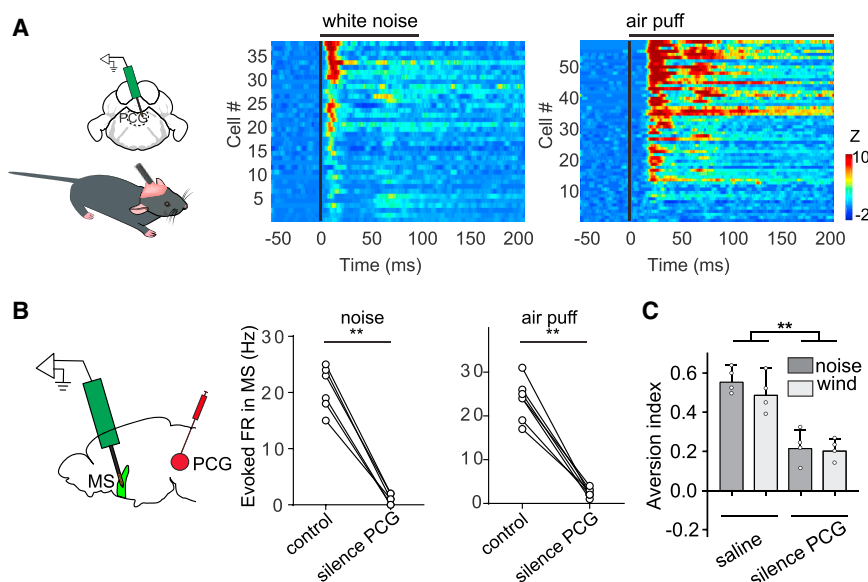
(legend continued on next page)

populations. In addition, axons from the POA-projecting MS neurons were not observed in LHb (Figure S7B), further suggesting a lack of collateralization of these neurons to the secondary target of interest. These results well explain the observation that stimulation of MS-to-POA axon terminals induced a speed increase whereas that of MS-to-LHb terminals did not.

To further confirm the involvement of the MS-to-POA projection in the locomotion effect, we injected AAV encoding Cre-dependent DREADDi in the MS of VGluT2-Cre mice. The DREADDi agonist clozapine-N-oxide (CNO) was infused locally to LHb or POA to silence the MS projections to these targets separately (Figure 6F). We found that silencing the MS-to-LHb projection impaired the noise-induced aversion (Figure 6G), while silencing the MS-to-POA projection reduced the increase of locomotion speed in the stimulation chamber (Figure 6H). These data confirm that the MS-to-LHb projection mediates the signaling of negative valence while the MS-to-POA projection promotes locomotion.

Finally, we analyzed the locomotion pattern in the stimulation chamber (Figure 6I). For the first five entries, the EYFP control animals spent about the same amount of time in the stimulation chamber in each trial (Figure 6J, blue). Animals with glutamatergic MS neurons stimulated stayed in the stimulation chamber for a shorter period of time than the control animals even for the first trial, and the time staying became shorter and shorter with the increasing number of trials (Figure 6J, orange). Animals with glutamatergic MS-to-LHb axon terminals stimulated initially stayed for a similar period as the control animals, but the time staying quickly reduced over the increasing number of trials and became comparable to stimulating MS neuron cell bodies (Figure 6J, gray). The average locomotion speed by stimulating MS-to-LHb axon terminals was initially similar to that in control yet lower

than stimulating MS neuron cell bodies, but it was gradually picked up with the increasing number of trials (Figure 6K). These results suggest that: (1) the negative valence signaled by the MS-to-LHb projection may require some accumulation time to have a behavioral effect, which becomes enhanced through repeated learning; and (2) the locomotion effect mediated by the MS-to-POA projection facilitates the animal's quick avoidance from the non-preferred environment upon initial contacts. Through learning, plastic changes might occur at some neuronal sites such that the enhanced locomotion could be achieved independent of the MS-to-POA projection.

A Bottom-Up Multisensory Pathway to Mediate Aversion
Previously, we have reported that, along the reticular-limbic auditory pathway, the pontine central gray (PCG) provides auditory input to the MS (Zhang et al., 2018). Using single-unit recordings, we further discovered that PCG neurons responded not only to high-intensity noise but also to air puffs (Figure 7A). In addition, silencing PCG with muscimol (Figure S8) eliminated both the auditory and the somatosensory responses recorded in the MS (Figure 7B). Moreover, silencing PCG greatly reduced the aversion caused by high-intensity noise and wind blows (Figure 7C). These data indicate that MS receives multisensory aversive signals via a bottom-up neural pathway mediated through PCG and then transmits these signals to LHb to generate aversion.

DISCUSSION

In this study, we have revealed a bottom-up multisensory neural pathway feeding input to LHb to generate sensory-evoked aversion (Figure 8). PCG in the pontine receives both auditory and somatosensory aversive signals and transmits them directly to the MS in the basal forebrain, a component of the limbic system. The MS further conveys the signals to LHb to produce negative emotions and behavioral avoidance. In the meantime, the MS

(I) Movement tracking for three example animals during the first, third, and fifth entry trials.

(J) Average time staying in the stimulation chamber for different entry trials in EYFP control (blue), and animals with MS neuron cell bodies (orange) or MS-to-LHb axon terminals (gray) stimulated. Bar, SD.

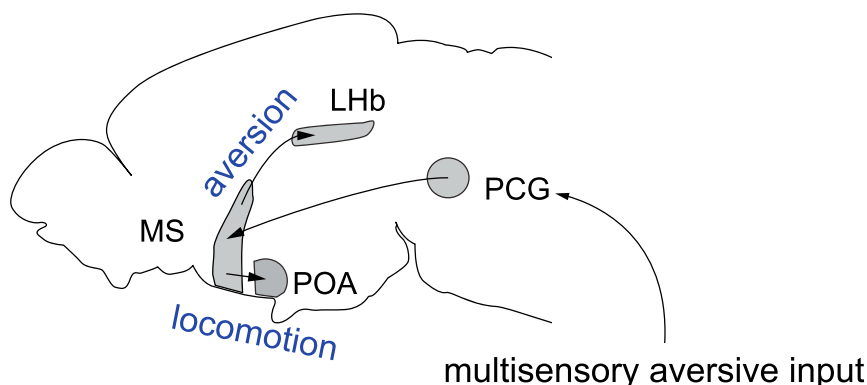(K) Average speed in the stimulation chamber for different entry trials.

Figure 8. A Proposed Circuit Model
Schematic illustration of a bottom-up multisensory neural pathway from PCG to MS and then to LHb (which mediates aversion) and POA (which mediates enhancement of locomotion).

transmits the signals to POA in the hypothalamus, leading to the enhancement of locomotion. Therefore, both emotional and motional effects are generated via the MS, allowing the animal to efficiently avoid aversive environments upon initial contacts.

Previously, studies related to the MS have mostly been focused on its projections to the hippocampus and EC and suggested MS involvement in arousal, attention, sensory gating, learning and memory, and navigation (Baxter and Chiba, 1999; Fuhrmann et al., 2015; Hasselmo, 2006; Robinson et al., 2016; Weber and Dan, 2016; Winson, 1978; Xu et al., 2015; Zhang et al., 2018). In the present study, we have elucidated a previously unrecognized functional role of the MS. Our data suggest that the MS may serve as an important multisensory center for transforming sensory cues into behavioral aversion. We show that MS neurons respond robustly to aversive sensory stimulation such as high-intensity noise and air puffs, but not to non-aversive stimuli such as tones (Figure S2A), although at extremely high intensities (e.g., ≥90 dB SPL), weak responses to tones can be observed (Zhang et al., 2018). This specificity suggests that MS conveys valence rather than salience information and that the PCG-MS-LHb pathway is a hard-wired circuit for signaling innately aversive sensory cues. It remains possible that this pathway can also convey conditioned aversive sensory cues, since conditioning-induced increases of auditory cue (tone) responses have been observed in LHb (Wang et al., 2017). This issue warrants extensive studies in the future.

The emotional function of the MS is achieved mainly through its glutamatergic projection to LHb. In the brain system processing aversive and reward signals, LHb has been shown to be important for signaling negative motivational valence (Matsumoto and Hikosaka, 2007; Namboodiri et al., 2016; Stamatakis and Stuber, 2012; Stephenson-Jones et al., 2016; Wang et al., 2017; Zhang et al., 2016). Previously, top-down influences have often been considered for modulating this system. For example, it has been suggested that LHb receives input from the limbic forebrain and modulates midbrain nuclei involved in reward, such as the ventral tegmental area (VTA) and substantia nigra pars compacta (SNc) (Gao et al., 1990; Herkenham and Nauta, 1979; Lammel et al., 2012; Stamatakis and Stuber, 2012; Kim and Lee, 2012). Although LHb neurons have been reported to respond to aversive events (Barker et al., 2017; Matsumoto and Hikosaka, 2007; Wang et al., 2017), how sensory cues are transmitted to LHb remains not well understood. In the pre-

sent study, we provide direct evidence that PCG conveys sensory input to the MS. PCG neurons are themselves multisensory (Figure 7) and receive sensory inputs from the caudal pontine reticular nucleus (Zhang et al., 2018). The latter receives somatosensory input from the spinal cord and auditory input from the cochlear nucleus (Willis, 2008; Koch, 1999). Thus, our study here suggests a bottom-up multisensory neural pathway leading up to LHb. Since there are multiple potential sources of sensory input to LHb (Barker et al., 2017; Golden et al., 2016; Lecca et al., 2017; Stephenson-Jones et al., 2016; Shabel et al., 2012; Hong and Hikosaka, 2008), we postulate that these different pathways may function independently or synergistically to mediate negative emotions under different environmental or behavioral contexts.

Notably, both glutamatergic and GABAergic MS neurons project to LHb, and these two projections can converge onto single LHb neurons. Therefore, activation of glutamatergic and GABAergic MS neurons separately produces opposite behavioral effects: place avoidance and place preference, respectively. These parallel, opposing pathways suggest that MS might be capable of modulating LHb bidirectionally, generating both negative and positive valence depending on the context (Matsumoto and Hikosaka, 2007; Wang et al., 2017). For the aversive stimuli tested in this study, glutamatergic MS neurons respond faster and more strongly than the GABAergic neurons, thus generating a net effect of negative valence. The role of GABAergic MS projection to LHb remains to be further explored in the future. Besides providing feedforward inhibition by the GABAergic input to balance excitation in LHb, some rewarding stimuli might be able to preferentially activate GABAergic MS neurons, thus inhibiting LHb and producing a net effect of positive valence.

Previously, the MS has been strongly linked to locomotor behavior. Either the firing rate or the frequency of theta rhythmic activity of MS neurons is modulated as a function of running speed (King et al., 1998; Zhou et al., 1999; Welday et al., 2011). Therefore, MS activity has been thought to encode velocity and provide this information to the hippocampus and EC (Fuhrmann et al., 2015; Hinman et al., 2016; Justus et al., 2017). In addition, optogenetic stimulation of glutamatergic MS neurons has been shown to induce running behavior (Fuhrmann et al., 2015; Justus et al., 2017). In the present study, using cell-type- and projection-specific manipulations, we have identified that the locomotion effect of stimulating glutamatergic MS neurons is mediated by their projections to POA. The resulting enhanced locomotion can facilitate efficient avoidance from the aversive environment upon initial contacts. Together, activation of the MS by sensory cues can generate concurrent emotional and motional outputs, which endow animals with an

innate capability to effectively avoid unpleasant or discomforting environments and pursue better-quality life, a fundamental survival strategy likely acquired through evolution.

STAR★METHODS

Detailed methods are provided in the online version of this paper and include the following:

- KEY RESOURCES TABLE
- CONTACT FOR REAGENT AND RESOURCE SHARING
- EXPERIMENTAL MODELS AND SUBJECT DETAILS
- METHOD DETAILS
  - Awake Head-Fixed Animal Preparation
  - Viral Injection
  - Optogenetic Manipulation
  - Pharmacological Manipulation
  - Cell-type-Specific Ablation
  - Chemogenetic Silencing
  - Sound Generation
  - Air Puff Stimulation
  - Electrophysiological Recording and Spike Sorting
  - Optrode Recording
  - Slice Recording
  - Analysis of Axon Collateralization
  - Image Acquisition
  - Behavioral Tests
  - Real-Time Mouse Detection
- QUANTIFICATION AND STATISTICAL ANALYSIS
  - Data Analysis
  - Statistics
- DATA AND SOFTWARE AVAILABILITY

SUPPLEMENTAL INFORMATION

Supplemental Information includes eight figures and seven videos and can be found with this article online at https://doi.org/10.1016/j.neuron.2018.07.023.

AUTHOR CONTRIBUTIONS

H.W.T. and L.I.Z. conceived the study. G.-W.Z. performed behavioral assays. L.S. performed *in vivo* multichannel recordings and data analysis. W.Z. performed slice recordings. H.W.T., L.I.Z., and Y.X. supervised the project. H.W.T., L.I.Z., and G.-W.Z. wrote the manuscript.

DECLARATION OF INTERESTS

The authors declare no competing interests.

REFERENCES

Aizawa, H., Kobayashi, M., Tanaka, S., Fukai, T., and Okamoto, H. (2012). Molecular characterization of the subnuclei in rat habenula. J. Comp. Neurol. *520*, 4051–4066.

Baker, P.M., Jhou, T., Li, B., Matsumoto, M., Mizumori, S.J.Y., Stephenson-Jones, M., and Vicentic, A. (2016). The Lateral habenula circuitry: reward processing and cognitive control. J. Neurosci. *36*, 11482–11488.

Barker, D.J., Miranda-Barrientos, J., Zhang, S., Root, D.H., Wang, H.L., Liu, B., Calipari, E.S., and Morales, M. (2017). Lateral preoptic control of the lateral habenula through convergent glutamate and GABA transmission. Cell Rep. *21*, 1757–1769.

Baxter, M.G., and Chiba, A.A. (1999). Cognitive functions of the basal forebrain. Curr. Opin. Neurobiol. *9*, 178–183.

Berridge, K.C., and Kringelbach, M.L. (2015). Pleasure systems in the brain. Neuron *86*, 646–664.

Boyden, E.S., Zhang, F., Bamberg, E., Nagel, G., and Deisseroth, K. (2005). Millisecond-timescale, genetically targeted optical control of neural activity. Nat. Neurosci. *8*, 1263–1268.

Chou, X.L., Wang, X., Zhang, Z.G., Shen, L., Zingg, B., Huang, J., Zhong, W., Mesik, L., Zhang, L.I., and Tao, H.W. (2018). Inhibitory gain modulation of defense behaviors by zona incerta. Nat. Commun. *9*, 1151.

Colom, L.V., Castaneda, M.T., Reyna, T., Hernandez, S., and Garrido-Sanabria, E. (2005). Characterization of medial septal glutamatergic neurons and their projection to the hippocampus. Synapse *58*, 151–164.

Crawley, J.N. (1985). Exploratory behavior models of anxiety in mice. Neurosci. Biobehav. Rev. *9*, 37–44.

Dong, H.-W. (2007). The Allen Reference Atlas: A Digital Color Brain Atlas Of The C57BL/6J Male Mouse (John Wiley and Sons).

Etkin, A., Büchel, C., and Gross, J.J. (2015). The neural bases of emotion regulation. Nat. Rev. Neurosci. *16*, 693–700.

Fadok, J.P., Krabbe, S., Markovic, M., Courtin, J., Xu, C., Massi, L., Botta, P., Bylund, K., Müller, C., Kovacevic, A., et al. (2017). A competitive inhibitory circuit for selection of active and passive fear responses. Nature *542*, 96–100.

Freund, T.F., and Antal, M. (1988). GABA-containing neurons in the septum control inhibitory interneurons in the hippocampus. Nature *336*, 170–173.

Fuhrmann, F., Justus, D., Sosulina, L., Kaneko, H., Beutel, T., Friedrichs, D., Schoch, S., Schwarz, M.K., Fuhrmann, M., and Remy, S. (2015). Locomotion, theta oscillations, and the speed-correlated firing of hippocampal neurons are controlled by a medial septal glutamatergic circuit. Neuron *86*, 1253–1264.

Gao, D.M., Jeaugey, L., Pollak, P., and Benabid, A.L. (1990). Intensity-dependent nociceptive responses from presumed dopaminergic neurons of the substantia nigra, pars compacta in the rat and their modification by lateral habenula inputs. Brain Res. *529*, 315–319.

Golden, S.A., Heshmati, M., Flanigan, M., Christoffel, D.J., Guise, K., Pfau, M.L., Aleyasin, H., Menard, C., Zhang, H., Hodes, G.E., et al. (2016). Basal forebrain projections to the lateral habenula modulate aggression reward. Nature *534*, 688–692.

Hasselmo, M.E. (2006). The role of acetylcholine in learning and memory. Curr. Opin. Neurobiol. *16*, 710–715.

Herkenham, M., and Nauta, W.J.H. (1979). Efferent connections of the habenular nuclei in the rat. J. Comp. Neurol. *187*, 19–47.

Hikosaka, O. (2010). The habenula: from stress evasion to value-based decision-making. Nat. Rev. Neurosci. *11*, 503–513.

Hinman, J.R., Brandon, M.P., Climer, J.R., Chapman, G.W., and Hasselmo, M.E. (2016). Multiple running speed signals in medial entorhinal cortex. Neuron *91*, 666–679.

Hong, S., and Hikosaka, O. (2008). The globus pallidus sends reward-related signals to the lateral habenula. Neuron *60*, 720–729.

Hu, H. (2016). Reward and aversion. Annu. Rev. Neurosci. *39*, 297–324.

Ji, H., and Shepard, P.D. (2007). Lateral habenula stimulation inhibits rat midbrain dopamine neurons through a GABA(A) receptor-mediated mechanism. J. Neurosci. 27, 6923–6930.

Justus, D., Dalügge, D., Bothe, S., Fuhrmann, F., Hannes, C., Kaneko, H., Friedrichs, D., Sosulina, L., Schwarz, I., Elliott, D.A., et al. (2017). Glutamatergic synaptic integration of locomotion speed via septoentorhinal projections. Nat. Neurosci. 20, 16–19.

Kim, U., and Lee, T. (2012). Topography of descending projections from anterior insular and medial prefrontal regions to the lateral habenula of the epithalamus in the rat. Eur. J. Neurosci. 35, 1253–1269.

King, C., Recce, M., and O'Keefe, J. (1998). The rhythmicity of cells of the medial septum/diagonal band of Broca in the awake freely moving rat: relationships with behaviour and hippocampal theta. Eur. J. Neurosci. 10, 464–477.

Koch, M. (1999). The neurobiology of startle. Prog. Neurobiol. 59, 107–128.

Kringelbach, M.L. (2016). Limbic cortex: the functional neuroanatomy of emotion and hedonic processing. In Neuroscience in the 21st Century: From Basic to Clinical, Second Edition, D.W. Pfaff and N.D. Volkow, eds. (Springer), pp. 1469–1501.

Lammel, S., Lim, B.K., Ran, C., Huang, K.W., Betley, M.J., Tye, K.M., Deisseroth, K., and Malenka, R.C. (2012). Input-specific control of reward and aversion in the ventral tegmental area. Nature 491, 212–217.

Lammel, S., Lim, B.K., and Malenka, R.C. (2014). Reward and aversion in a heterogeneous midbrain dopamine system. Neuropharmacology 76 (Pt B), 351–359.

Lecca, S., Meye, F.J., and Mameli, M. (2014). The lateral habenula in addiction and depression: an anatomical, synaptic and behavioral overview. Eur. J. Neurosci. 39, 1170–1178.

Lecca, S., Meye, F.J., Trusel, M., Tchenio, A., Harris, J., Schwarz, M.K., Burdakov, D., Georges, F., and Mameli, M. (2017). Aversive stimuli drive hypothalamus-to-habenula excitation to promote escape behavior. eLife 6, 6.

LeDoux, J. (2012). Rethinking the emotional brain. Neuron 73, 653–676.

Li, B., Piriz, J., Mirrione, M., Chung, C., Proulx, C.D., Schulz, D., Henn, F., and Malinow, R. (2011). Synaptic potentiation onto habenula neurons in the learned helplessness model of depression. Nature 470, 535–539.

Li, X., Yu, B., Sun, Q., Zhang, Y., Ren, M., Zhang, X., Li, A., Yuan, J., Madisen, L., Luo, Q., et al. (2018). Generation of a whole-brain atlas for the cholinergic system and mesoscopic projectome analysis of basal forebrain cholinergic neurons. Proc. Natl. Acad. Sci. USA 115, 415–420.

Liang, F., Xiong, X.R., Zingg, B., Ji, X.Y., Zhang, L.I., and Tao, H.W. (2015). Sensory cortical control of a visually induced arrest behavior via corticotectal projections. Neuron 86, 755–767.

Matsumoto, M., and Hikosaka, O. (2007). Lateral habenula as a source of negative reward signals in dopamine neurons. Nature 447, 1111–1115.

Matsumoto, M., and Hikosaka, O. (2009). Representation of negative motivational value in the primate lateral habenula. Nat. Neurosci. 12, 77–84.

Mercer, L.F., Jr., and Remley, N.R. (1979). Mapping of sensory-responsive cells in the septal area of the rat. Brain Res. Bull. 4, 483–490.

Miller, C.L., and Freedman, R. (1993). Medial septal neuron activity in relation to an auditory sensory gating paradigm. Neuroscience 55, 373–380.

Namboodiri, V.M., Rodriguez-Romaguera, J., and Stuber, G.D. (2016). The habenula. Curr. Biol. 26, R873–R877.

Petreanu, L., Mao, T., Sternson, S.M., and Svoboda, K. (2009). The subcellular organization of neocortical excitatory connections. Nature 457, 1142–1145.

Proulx, C.D., Hikosaka, O., and Malinow, R. (2014). Reward processing by the lateral habenula in normal and depressive behaviors. Nat. Neurosci. 17, 1146–1152.

Robinson, J., Manseau, F., Ducharme, G., Amilhon, B., Vigneault, E., El Mestikawy, S., and Williams, S. (2016). Optogenetic activation of septal glutamatergic neurons drive hippocampal theta rhythms. J. Neurosci. 36, 3016–3023.

Rossant, C., Kadir, S.N., Goodman, D.F.M., Schulman, J., Hunter, M.L.D., Saleem, A.B., Grosmark, A., Belluscio, M., Denfield, G.H., Ecker, A.S., et al. (2016). Spike sorting for large, dense electrode arrays. Nat. Neurosci. 19, 634–641.

Saunders, A., Granger, A.J., and Sabatini, B.L. (2015). Corelease of acetylcholine and GABA from cholinergic forebrain neurons. eLife 4, 4.

Schmitzer-Torbert, N., Jackson, J., Henze, D., Harris, K., and Redish, A.D. (2005). Quantitative measures of cluster quality for use in extracellular recordings. Neuroscience 131, 1–11.

Shabel, S.J., Proulx, C.D., Trias, A., Murphy, R.T., and Malinow, R. (2012). Input to the lateral habenula from the basal ganglia is excitatory, aversive, and suppressed by serotonin. Neuron 74, 475–481.

Stamatakis, A.M., and Stuber, G.D. (2012). Activation of lateral habenula inputs to the ventral midbrain promotes behavioral avoidance. Nat. Neurosci. 15, 1105–1107.

Stephenson-Jones, M., Yu, K., Ahrens, S., Tucciarone, J.M., van Huijstee, A.N., Mejia, L.A., Penzo, M.A., Tai, L.H., Wilbrecht, L., and Li, B. (2016). A basal ganglia circuit for evaluating action outcomes. Nature 539, 289–293.

Tervo, D.G.R., Hwang, B.Y., Viswanathan, S., Gaj, T., Lavzin, M., Ritola, K.D., Lindo, S., Michael, S., Kuleshova, E., Ojala, D., et al. (2016). A designer AAV variant permits efficient retrograde access to projection neurons. Neuron 92, 372–382.

Vankov, A., Hervé-Minvielle, A., and Sara, S.J. (1995). Response to novelty and its rapid habituation in locus coeruleus neurons of the freely exploring rat. Eur. J. Neurosci. 7, 1180–1187.

Viola, P., and Jones, M. (2001). Rapid object detection using a boosted cascade of simple features. Proceedings of 2001 IEEE Computer Society Conference on Computer Vision and Pattern Recognition 1, 511–518.

Wang, D., Li, Y., Feng, Q., Guo, Q., Zhou, J., and Luo, M. (2017). Learning shapes the aversion and reward responses of lateral habenula neurons. eLife 6, 6.

Weber, F., and Dan, Y. (2016). Circuit-based interrogation of sleep control. Nature 538, 51–59.

Welday, A.C., Shlifer, I.G., Bloom, M.L., Zhang, K., and Blair, H.T. (2011). Cosine directional tuning of theta cell burst frequencies: evidence for spatial coding by oscillatory interference. J. Neurosci. 31, 16157–16176.

Willis, W.D. (2008). Physiological characteristics of second-order somatosensory circuits in spinal cord and brainstem. In The Senses: A Comprehensive Reference, Volume 6, A.I. Basbaum, A. Kaneko, G.G. Shepherd, G. Westheimer, E. Gardner, and J.H. Kaas, eds. (Academic Press), pp. 87–116.

Winson, J. (1978). Loss of hippocampal theta rhythm results in spatial memory deficit in the rat. Science 201, 160–163.

Xiong, X.R., Liang, F., Zingg, B., Ji, X.Y., Ibrahim, L.A., Tao, H.W., and Zhang, L.I. (2015). Auditory cortex controls sound-driven innate defense behaviour through corticofugal projections to inferior colliculus. Nat. Commun. 6, 7224.

Xu, M., Chung, S., Zhang, S., Zhong, P., Ma, C., Chang, W.C., Weissbourd, B., Sakai, N., Luo, L., Nishino, S., and Dan, Y. (2015). Basal forebrain circuit for sleep-wake control. Nat. Neurosci. 18, 1641–1647.

Yang, C.F., Chiang, M.C., Gray, D.C., Prabhakaran, M., Alvarado, M., Juntti, S.A., Unger, E.K., Wells, J.A., and Shah, N.M. (2013). Sexually dimorphic neurons in the ventromedial hypothalamus govern mating in both sexes and aggression in males. Cell 153, 896–909.

Zaborszky, L., van den Pol, A.N., and Gyengesi, E. (2012). The basal forebrain cholinergic projection system in mice. In The Mouse Nervous System, C. Watson, G. Paxinos, and L. Puelles, eds. (Academic Press), pp. 684–718.

Zhang, J., Tan, L., Ren, Y., Liang, J., Lin, R., Feng, Q., Zhou, J., Hu, F., Ren, J., Wei, C., et al. (2016). Presynaptic excitation via GABAB receptors in habenula cholinergic neurons regulates fear memory expression. Cell 166, 716–728.

Zhang, G.-W., Sun, W.-J., Zingg, B., Shen, L., He, J., Xiong, Y., Tao, H.W., and Zhang, L.I. (2018). A non-canonical reticular-limbic central auditory

pathway via medial septum contributes to fear conditioning. Neuron *97*, 406–417.e4.

Zhou, T.L., Tamura, R., Kuriwaki, J., and Ono, T. (1999). Comparison of medial and lateral septal neuron activity during performance of spatial tasks in rats. Hippocampus *9*, 220–234.

Zhu, H., and Roth, B.L. (2014). Silencing synapses with DREADDs. Neuron *82*, 723–725.

Zhu, Y., Wienecke, C.F.R., Nachtrab, G., and Chen, X. (2016). A thalamic input to the nucleus accumbens mediates opiate dependence. Nature *530*, 219–222.

Zingg, B., Chou, X.L., Zhang, Z.G., Mesik, L., Liang, F., Tao, H.W., and Zhang, L.I. (2017). AAV-mediated anterograde transsynaptic tagging: mapping corti-cocollicular input-defined neural pathways for defense behaviors. Neuron *93*, 33–47.

STAR★METHODS

KEY RESOURCES TABLE

REAGENT or RESOURCE	SOURCE	IDENTIFIER
Antibodies		
Fluorescent Nissl Stain	Invitrogen	RRID: AB_2572212
Bacterial and Virus Strains		
AAV9.EF1α.DIO.hChR2(H134R)-EYFP.WPRE.hGH	A gift from Karl Deisseroth	Addgene plasmid# 20298
pAAV-Syn-GFP	A gift from Edward Boyden	Addgene plasmid# 58867
AAVretro-GFP, AAVretro-Cre	Tervo et al., 2016	N/A
ΔG-rabies-GFP	Salk Institute	N/A
rAAV5/hsyn-con/Foff-hChR2(H134R)-EYFP-WPRE	A gift from Karl Deisseroth	Addgene plasmid# 55645
AAV1-EF1α-DIO-EYFP	A gift from Karl Deisseroth	Addgene plasmid# 27056
rAAV1/Flex-taCasp3-TEVP	A gift from Nirao Shah & Jim Wells	Addgene plasmid# 45580
AAV-EF1α-DIO-h4MDi-mCherry	A gift from Bryan Roth	Addgene plasmid# 50461
AAV- EF1α-DIO-mCherry	A gift from Bryan Roth	Addgene plasmid# 50462
AAV1-EF1α-DIO-Flp	custom design, ViGene Biosciences	N/A
AAVDJ-EF1α-fDIO-YFP	UNC Vector Core	N/A
Chemicals, Peptides, and Recombinant Proteins		
Kwik-Cast Sealant	WPI, Inc.	KWIK-CAST
DiI	Invitrogen	D282
Paraformaldehyde	Alfa Aesar	10194340
NaCl	OmniPur	UI27FZEMS
KCl	Mallinckrodt	7447-40-7
$NaHCO_3$	EMD Chemicals	48204847
$MgCl_2$	J.T. Baker	7791-18-6
$CaCl_2$	EMD Chemicals	41046444
Glucose	Sigma	SLBC6575V
Sucrose	Millipore	D00168514
Agarose	OmniPur	3332C511
Muscimol, >98%; Tocris; 10 mg	Fisher Scientific	28910
Clozapine-N-oxide	Tocris	34233-69-7
Experimental Models: Organisms/Strains		
Mouse: C57BL/6J	The Jackson Laboratory	RRID: IMSR_JAX:000664
Mouse: Ai14	The Jackson Laboratory	RRID: IMSR_JAX:007914
Mouse: VGluT2-ires-Cre mice	The Jackson Laboratory	RRID: IMSR_JAX: 016963
Mouse: GAD2-ires-Cre mice	The Jackson Laboratory	RRID: IMSR_JAX: 010802
Mouse: ChAT-ires-Cre mice	The Jackson Laboratory	RRID: IMSR_JAX: 028861
Software and Algorithms		
Data acquisition with LabVIEW	LabVIEW	http://www.ni.com/en-us/shop/labview.html; RRID: SCR_014325
Custom-written MATLAB code for analysis	MATLAB	https://www.mathworks.com/; RRID: SCR_001622
Allen Reference Atlas	Dong, 2007	http://www.brain-map.org; RRID: SCR_008848
Mclust	A.D. Redish	http://redishlab.neuroscience.umn.edu/MClust/MClust.html
Offline sorter	Plexon	https://plexon.com; RRID: SCR_000012

(Continued on next page)

Continued

REAGENT or RESOURCE	SOURCE	IDENTIFIER
Prism	GraphPad	https://www.graphpad.com/scientific-software/prism/; RRID: SCR_002798
Fiji	NIH	https://fiji.sc/; RRID: SCR_002285
Custom-written python code for analysis	Python	https://www.python.org/; RRID:SCR_008394
OpenCV library	OpenCV	https://opencv.org/; RRID: SCR_015526
Other		
Free Field Speaker	Vifa XT25G30-04 1″ Dual Ring Tweeter	N/A
Sound-Attenuation Booth	Gretch-Ken Industries	N/A
NI board for sound generation	National Instrument	PCI-6731
Optrode	Neuronexus Technologies	A1x16-Poly2-5mm-50 s-177-OA16LP
Multi-channel silicone probe	Neuronexus Technologies	A1x32-poly2-6mm-23 s
Microvalve	Lee Co.	LFAA1209512H

CONTACT FOR REAGENT AND RESOURCE SHARING

Further information and requests for resources and reagents should be directed to and will be fulfilled by the Lead Contact, Huizhong W. Tao (htao@usc.edu).

EXPERIMENTAL MODELS AND SUBJECT DETAILS

Experiments were carried out in the Zilkha Neurogenetic Institute of the University of Southern California (USC). All experimental procedures in this study were approved by the Animal Care and Use Committee of USC. The VGluT2-ires-Cre (RRID: IMSR_JAX: 016963), GAD2-ires-Cre (RRID: IMSR_JAX: 010802), ChAT-ires-Cre (RRID: IMSR_JAX: 028861), Ai14 (Cre-dependent tdTomato reporter line; RRID: IMSR_JAX:007914), and wild-type C57BL/6J (RRID: IMSR_JAX:000664) mice were obtained from the Jackson Laboratory. Mice were housed in a 12h light-dark cycle (lights on 20:00 and off at 8:00) with free access to food and water. Experiments were performed in adult male and female mice (6-10 weeks old).

METHOD DETAILS

Awake Head-Fixed Animal Preparation

The mouse was anesthetized with isoflurane (1.5%–2% by volume), and a head post for fixation was mounted on top of the skull with dental cement and a craniotomy was performed over the intended recording region (MS: 0.9 mm anterior than the bregma, 1 mm lateral to the midline, 4.2-5 mm below the pia with a 13° angle; LHb: 1.5 mm posterior than the bregma, 1mm to the midline, 2.5 mm below the pia with a 10° angle; PCG: 5.5 mm posterior to bregma, 0.5 mm lateral to midline, 3.5 mm below the pia) three days before the recording. Silicone adhesive (Kwik-Cast Sealant, WPI Inc.) was applied to cover the craniotomy window until the recording experiment. The animal was trained to run freely on a running plate during the recovery period.

Viral Injection

AAV9.EF1α.DIO.hChR2(H134R)-EYFP.WPRE.hGH (UPenn vector core, Addgene 20298), rAAV5/hsyn-con/Foff-hChR2(H134R)-EYFP-WPRE (UNC GTC vector core, Addgene 55645), AAV1-EF1α-DIO-EYFP (UPenn vector core, Addgene 27056), rAAV1/Flex-taCasp3-TEVP (UNC GTC vector core, Addgene 45580), AAVretro-GFP, AAVretro-Cre (Tervo et al., 2016), AAV-EF1α-DIO-h4MDi-mCherry (Addgene 50461) and AAV-EF1α-DIO-mCherry (Addgene 50462), AAV1-EF1α-DIO-Flp (1.5 × 10^{14} GC/ml, custom design, ViGene Biosciences), AAVDJ-EF1α-fDIO-YFP (UNC Vector Core, 1.6 × 10^{13} GC/ml) were used in this study. Stereotaxic injection of the virus was carried out as we previously described (Zhang et al., 2018; Zingg et al., 2017). Coordinates for injections followed those for recording. Mice were anesthetized with 1.5% isoflurane. A small cut was made on the skin and the muscles were removed. One ~0.2-mm craniotomy window was made for each region. The adeno-associated viruses (AAVs, encoding ChR2, Caspase-3, hM4Di, Cre, mCherry or EYFP) were used depending on the purpose of experiments and strain of mice. A beveled glass micropipette (tip diameter: ~20 μm) was used to deliver the virus, and the glass micropipette was attached to a microsyringe pump (World Precision Instruments). For each injection, 60 nL of the viral solution was injected at a rate of 15 nL min^{-1}. Right after the injection, the pipette was allowed to rest for 5 min before withdrawal. The scalp was then sutured. Following the surgery, 0.1 mg kg^{-1} buprenorphine was injected subcutaneously before returning the animals to their home cages. Mice were allowed to recover for at least 3 weeks before behavioral or recording experiments. After each experiment, the brain was sectioned and imaged under a confocal microscope to confirm viral expression.

Optogenetic Manipulation

Animals were anesthetized with isoflurane and optic cannula (200 μm, Thorlabs) was stereotaxically implanted into the targeted region depending on the purpose of the experiments (MS, unilateral implantation; LHb, bilateral implantation; POA, bilateral implantation, 0.1 mm anterior to the bregma, 2 mm lateral to the midline, 5.3 mm below the pia with a 15° angle; dHipp, bilateral implantation, 3 mm posterior to the bregma, 2.7 mm to the midline, 2 mm below the pia; vHipp, bilateral implantation, 3.3 mm posterior to the bregma, 3.3 mm to the midline, 3.6 mm below the pia; LHA, bilateral implantation, 2 mm posterior to the bregma, 1 mm to the midline, 4.7 mm below the pia; EC, bilateral implantation, 4.7 mm posterior to the bregma, 3.2 mm to the midline, 2.6 mm below the pia). The optic cannula was fixed with dental cement, and a head post was mounted on top of the skull for animals on treadmill running tests. The mice were allowed to recover for at least 1 week before the behavior tests. During 3-days before behavioral tests, animals were connected to optical fibers without LED stimulation for habituation. On the test day, the optic fiber (200 μm core, NA 0.22, Thorlabs) was connected to a blue LED source (480 nm, 20Hz, 20-ms duration, Thorlabs) for stimulation. The power of LED light delivered to ferrule was controlled at ∼10 mW. After each experiment, the brain was sectioned and imaged under a confocal microscope to confirm the implantation site.

Pharmacological Manipulation

Animals were anesthetized with isoflurane and a drug cannula (internal diameter: 140 μm) was stereotaxically implanted into target region based on the purpose the experiments. Fluorescent muscimol-bodipy (0.7 mM in ACSF with 5% DMSO) was applied via the implanted cannula ten mins before behavioral tests. The silencing efficiency was evaluated by comparing the evoked spike responses before and after the perfusion of the drug. For MS and POA silencing, 150 nL muscimol was perfused unilaterally. For LHb and PCG silencing, 100 nL muscimol (per hemisphere) was perfused bilaterally.

Cell-type-Specific Ablation

Cre-dependent caspase-3 virus was delivered by stereotaxically injecting rAAV1/Flex-taCasp3-TEVP into MS of VGluT2-Cre, GAD2-Cre or ChAT-Cre mice. Following 2 weeks post-surgery survival time, the animal underwent behavior tests, and then the brain was fixed and sectioned to evaluate the efficiency of cell ablation.

Chemogenetic Silencing

Virus encoding Cre-dependent inhibitory DREADD receptors (hM4Di) was stereotaxically injected into MS of VGluT2-Cre mice. For general MS inhibition, the DREADDi agonist, CNO, was administered (i.p., 1mg/kg) 20 min before the behavior test. For projection-specific inactivation, CNO (3μM, 200 nL) was infused through the implanted drug cannula 20 min before the behavioral test (Zhu et al., 2016; Barker et al., 2017). Viral expression and location of implantation were verified post hoc.

Sound Generation

For head-fixed mice, the position of an open field speaker (Vifa XT25G30-04 1'' Dual Ring Tweeter) was adjusted according to that of the ear, such that the speaker was always 10 cm away from and facing the left ear, with the ear canal aligned with the axis of the speaker. Software for sound stimulation and data acquisition was custom developed with LabVIEW (PCI-6731 NI board for sound generation, 16-bits output, 1MHz sampling rate, National Instruments, Austin, TX). 80 dB SPL white noise (50-ms duration, 50 trials, with 5 s inter-stimulus interval) were tested. For noise-induced place aversion, the speaker was hidden in a corner of the designated stimulation chamber. White noise (80 dB SPL) was continuously delivered. There was about 15-20 dB attenuation of the sound in the connected chamber.

Air Puff Stimulation

For head-fixed awake mice recoding, the air was provided by the center air with an internal pressure of around 40-44 psi. A microvalve (LFAA1209512H, Lee Co, ESSEX, CT) was used to control the delivery of the air puff. The port to deliver the air puff was positioned 10 cm away from and facing the back of the animal. For air-puff induced place aversion, a battery powered fan was used to deliver the continuous wind blow in the designated stimulation chamber.

Electrophysiological Recording and Spike Sorting

Multi-channel recording was carried out with a 16-channel silicone probe (A1x16-Poly2-5mm-50 s-177-A16, 16 contacts separated by 50 μm, Neuronexus Technologies) in head-fixed animals. Signals were recorded and filtered through a bandpass filter (0.3 - 3 kHz). The nearby four channels of the probe were grouped as tetrodes, and semiautomatic spike sorting was performed by using Offline Sorter (Plexon). Semiautomated clustering was carried out on the basis of the first three principal components of the spike waveform on each tetrode channel using a T-Dist E-M scan algorithm (scan over a range of 10-30 degree of freedom) and then evaluated with sort quality metrics. Clusters with isolation distance < 20 and L-Ratio > 0.1 were discarded (Rossant et al., 2016; Schmitzer-Torbert et al., 2005). Spike clusters were classified as single units only if the waveform SNR (Signal Noise Ratio) exceeded 4 (12 dB) and the inter-spike intervals exceeded 1.2 ms for >99.5% of the spikes. Recording in the freely moving animal was carried out with a 32-channel chronic silicone probe (A1x32-poly2-6mm-23 s, 32 contacts separated by 23 μm, NeuroNexus Technologies). The

data acquisition was accomplished by using the OpenEphys recording system with a 32-channel headstage (Intan). The recorded files were converted to binary format with 16-bit resolution and processed as described above.

Optrode Recording
The VGluT2- and GAD2-positive neurons were genetically tagged by injecting floxed-AAV-ChR2. The optrode (A1x16-Poly2-5mm-50 s-177-OA16LP, 16 contacts separated by 50 μm, the distance between the tip of the optic fiber and the probes is 200 μm, NA 0.22, Neuronexus Technologies) was connected to a LED light source (480nm, Thorlabs) with an optic fiber. To identify ChR2+ neurons, 16-Hz (5-ms pulse duration, 100 ms total duration, controlled via an Arduino microcontroller) and 32-Hz (5-ms pulse duration, 100 ms total duration) LED pulse trains were delivered intermittently. To assess whether these units were driven directly by ChR2 or indirectly by synaptic connections, we analyzed the onset latency relative to each light stimulation. Only spikes with latency < 3 ms were considered as being directly stimulated in this study. We analyzed the waveform similarity between LED-evoked and sound- or air puff-evoked spikes. The correlation coefficient was computed between the average waveforms of these laser-evoked spikes and the spontaneous spikes (Figure 4H).

Slice Recording
To confirm synaptic connectivity between MS and LHb, Cre-dependent AAV-ChR2 (60 nL in volume) was injected into MS of VGluT2-Cre or GAD2-Cre mice. Following a 4-week post-injection survival time, acute brain slices containing LHb were prepared. Following urethane anesthesia, the animal was decapitated and the brain was rapidly removed and immersed in an ice-cold dissection buffer (composition: 60 mM NaCl, 3 mM KCl, 1.25 mM NaH$_2$PO$_4$, 25 mM NaHCO$_3$, 115 mM sucrose, 10 mM glucose, 7 mM MgCl$_2$, 0.5 mM CaCl$_2$; saturated with 95% O$_2$ and 5% CO$_2$; pH = 7.4). Brain slices of 300 μm thickness containing the LHb were cut in a coronal plane using a vibrating microtome (Leica VT1000s). Slices were allowed to recover for 30 min in a submersion chamber filled with the warmed (35°C) ACSF and then to cool gradually to the room temperature until recording. The spatial expression pattern of ChR2-EYFP in each slice was examined under a fluorescence microscope before recording. Neurons in LHb were mostly glutamatergic neurons (Aizawa et al., 2012; Wang et al., 2017). Patch pipettes (Kimax) with ∼4-5 MΩ impedance were used for whole-cell recordings. Recording pipettes contained: 130 mM K-gluconate, 4 mM KCl, 2 mM NaCl, 10 mM HEPES, 0.2 mM EGTA, 4 mM ATP, 0.3 mM GTP, and 14 mM phosphocreatine (pH, 7.25; 290 mOsm). Signals were recorded with an Axopatch 200B amplifier (Molecular Devices) under voltage clamp mode at a holding voltage of –70 mV for excitatory currents and 0 mV for inhibitory currents, filtered at 2 kHz and sampled at 10 kHz. 1 μM tetrodotoxin (TTX) and 1 mM 4- aminopyridine (4-AP) was added to the external solution for recording only monosynaptic responses (Petreanu et al., 2009) to blue light stimulation (3-10 ms pulse, 3 mW power, 10-30 trials, delivered via a mercury Arc lamp gated with an electronic shutter). To test if MS provided monosynaptic excitatory input to LHb, glutamate receptor antagonist CNQX (20 μM, Sigma-Aldrich) was added to the bath solution following demonstration of LED-evoked synaptic responses in patched neurons. To determine if MS provided monosynaptic GABAergic input to LHb, GABAergic receptor antagonist Gabazine (20 μM, Sigma-Aldrich) was added. To determine if a single LHb neuron could receive both monosynaptic excitatory and inhibitory inputs, non-floxed AAV-ChR2 (60 nL in volume) was injected into MS of wild-type C57BL mice and recording was performed with TTX and 4-AP present in the external solution.

Analysis of Axon Collateralization
We exploited three methods to investigate the collateralization of LHb- and POA-projecting MS neurons: 1) AAVretro-GFP and AAV-retro-Cre (Tervo et al., 2016) were injected into LHb and POA respectively of an Ai14 mouse (Figure 6D), which could retrogradely label the populations projecting to the corresponding targets; 2) CTb-Alexa647 and CTb-Alexa488 (Invitrogen) were injected into LHb and POA respectively of a wild-type mouse (Figure S7A); 3) AAV-EF1α-DIO-flp was injected into POA of a VGlutT2-Cre mouse, which would be retrogradely transported (Zingg et al., 2017) to MS and allow expression of flippase (FLP) in glutamatergic MS neurons, and this was followed by injection of AAVDJ-EF1α-fDIO-YFP (UNC Vector Core) into MS, allowing FLP-dependent expression of YFP (Figure S7B).

Image Acquisition
To check the expression of EYFP, ChR2, mCherry, CTb Alexa488, CTb Alexa647 or electrode (coated with DiI) tracks and muscimol injection sites, the animals were deeply anesthetized using urethane (25%) and transcardially perfused with phosphate-buffered saline (PBS) and paraformaldehyde (4% in PBS). Coronal brain sections (150 μm) were made with a vibratome (Leica Microsystems) and stained with nissl reagent (Deep red, Invitrogen) for 2 hr at room temperature. Each slice was imaged under a confocal microscope (Olympus).

Behavioral Tests
Mice were handled for a week with a cup before behavioral experiments. All behavior tests were conducted in a sound attenuation booth during the dark cycle of the mice. All behavioral experiments were videotaped for offline analysis.
Head-Fixed Running Test
The mice were accustomed to the head-fixation on a smoothly rotatable plate attached onto an optical shaft digital encoder (H1, US Digital) (Xiong et al., 2015; Chou et al., 2018) for 3 days (20 min/per day). On the 4th day, the animals were first habituated for 5 mins

and LED stimulation of different frequencies (2Hz, 5Hz, 10Hz, 20Hz, 20-ms pulse duration) and total durations (5 s, 10 s, 15 s) was delivered under the control of customized LabVIEW software. The inter-stimulation interval is 3 min. Speed information was extracted from the encoder for offline analysis.

Real-Time Place Preference Test

A clear acrylic behavior box (40cm x 20cm x 20cm) with normal bedding materials was used. For each trial, the mouse was initially placed in the non-stimulation chamber, and 20Hz (20-ms pulse duration) LED stimulation was constantly delivered once the animal entered the stimulation chamber and was stopped when the animal exited (Stamatakis and Stuber, 2012). The total duration of each trial was 20 mins. Animals were returned to their home cage after each test session. The stimulation chamber was randomly assigned to each animal and balanced for the whole group. We recorded the behavioral data via a web camera. The online analysis is as described below.

Conditioned Place Preference Test

A clear acrylic behavior box (40cm x 20cm x 20cm) was divided into three chambers. The middle chamber has a gray smooth metal plate floor, the left chamber has white walls and a grid-wire floor, and the right chamber has black walls and a parallel-wire floor. On day 1, each animal was placed in the middle chamber, and no preference toward either left or right chamber was observed (Figure S3). The black or white chamber was then assigned randomly to the stimulation chamber for that animal. On the 2nd and 3rd day, the animal was confined to the stimulation chamber for 20 mins while LED stimulation was applied. And 4 hr later it was also placed in the other chamber with no treatment for 20 mins. On the 4th day, the animal was placed in the middle chamber and could freely get access to all chambers.

Exploration Test

A clear acrylic behavior box consisting of two chambers with a movable metal gate between the chambers was used. At the beginning of each test, the gate was closed and the animal was forced to stay in one chamber (home chamber) for 20 mins. Then the gate was opened, and the animal could freely get access to both chambers. Control animals would spend more time in the novel chamber for exploration.

Real-Time Mouse Detection

A customized mouse detection software (written by Guangwei Zhang, in Python 2.7, https://www.python.org) was based on Haar-like features (Viola and Jones, 2001). 2000 positive (C57BL mice) and negative images (random background images under our experimental conditions) were manually collected. The openCV2 (https://opencv.org) toolbox was used to train the object detection cascades for 11 rounds until the false detection rate was lower than 0.04% and hit rates higher than 99.99%. The behavior of the animal was monitored using a camera (Logitech) at 24 frames/sec. The classifier cascades were used to detect the center point of the animal in each frame and we used the heatmap (with 10x10 pixels two-dimensional smooth) to represent the spatial density of these dots (Figure S1). The stimulation chamber was randomly assigned (balanced within the group) to each animal. Once the mice entered the stimulation chamber, computer-controlled Arduino microcontroller (https://www.arduino.cc/) would generate 20Hz TTL signals to drive the LED light source (ThorLabs).

QUANTIFICATION AND STATISTICAL ANALYSIS

Data Analysis

For electrophysiological recording data, spike trains were offline sorted as described above and analyzed with customized MATLAB scripts (written by Li Shen, Mathworks). For pharmacological silencing experiments, same units before and after perfusion of muscimol were compared. The Z-score was calculated as the firing rate at each time point divided by the standard deviation of the baseline firing rate (calculated within a 50-ms window before the stimulus onset), with a 1-ms bin. For treadmill running test, the onset latency was determined as the first time point when the speed exceeded the baseline by three times standard deviation of the baseline speed. It should be noted that animals normally stayed still in the control state. Speed values were determined based on the encoder reading, using a scaling factor which is dependent on parameters such as cycles per revolution (CPR) and output rate of the encoder. Instantaneous speed was calculated from two sequential video frames.

Statistics

Pilot experiments were conducted to determine the sample size. One-way ANOVA and post hoc Tukey's multiple comparisons were used to test significance between samples. For two-group comparison, significance was determined by using t test. Paired t test was used to compare data from the same neuron or animal.

DATA AND SOFTWARE AVAILABILITY

The data and tracking software were available upon reasonable request to the corresponding authors. Please note that the trained classifier cascades have been optimized for our experimental conditions.